University of Baghdad
College of Engineering
JE
JOURNAL OF ENGINEERING

Journal of Engineering

journal homepage: www.jcoeng.edu.iq

Volume 32 Number 5 May 2026

Numerical Study of CFRP-Strengthened Square RC Columns under Axial Compression with Initial Geometric Imperfections

Ali Majid Mousa*, Salah R. Al Zaidee

Department of Civil Engineering, College of Engineering, University of Baghdad, Baghdad, Iraq

ABSTRACT

Reinforced concrete (RC) columns are the enablers of modern cities; their numerical modeling requires precise treatment of initial geometric imperfections and confinement effects to represent their structural behavior realistically. This study describes a finite element analysis (FEA) framework developed in Abaqus/CAE to investigate the axial behavior of full-scale short and slender square RC columns with and without interior transverse reinforcement (ties). The models include external confinement with carbon fiber–reinforced polymer (CFRP) jacketing, and different global and local imperfection cases were considered to assess their effects on strength and ductility. Calibration against code provisions was achieved by comparing the numerical results with an interaction diagram derived in accordance with ACI 318-25 and ACI PRC-440.2-23 design requirements. The study showed that as the imperfection amplitude increases, the strength and ductility of short, slender RC columns decrease, irrespective of confinement. For short columns subjected to axial compression, one can achieve good correlation with code-based nominal axial load predictions without considering explicit imperfections, provided no strength reduction factor is included, and accidental eccentricities are ignored. In contrast, for slender columns, imperfections are key in inducing slenderness effects, particularly in global imperfection cases with pinned-end boundary conditions.

Keywords: Axially loaded RC columns, CFRP jacketing, Code-based calibration, Finite element, Initial geometric imperfections.

1. INTRODUCTION

The construction of structural systems, as well as the fabrication and manufacturing of structural members, is subject to imperfections. The load-carrying capacity of compression-loaded structural elements is the most vulnerable to these imperfections; consequently, they should be accounted for in the design process and the resultant load-deflection curves **(Walport et al., 2020)**. Imperfections in structural columns typically originate from initial geometric or loading eccentricities, leading to premature bending under axial compression

*Corresponding author
Peer review under the responsibility of University of Baghdad.
https://doi.org/10.31026/j.eng.2026.05.05

Article received: 30/01/2026
Article revised: 05/04/2026
Article accepted: 14/04/2026
Article published: 01/05/2026

(Harvey and Cain, 2020). Research in literature has focused on the bearing capacity of compressed structural members with various forms of imperfections. These variations can initiate slopes that deviate from the design specification or become apparent over the structure's lifetime **(Alekseytsev and Kurchenko, 2023)**. **(Alekseytsev and Kurchenko, 2023)** studied the impact of initial imperfections and material degradation on the condition index of reinforced concrete (RC) columns subjected to emergency loads. Their study demonstrated that initial geometrical imperfections play a minor role in the total load-bearing capacity, even when sufficient safety margins are considered during the design process. Typically, a margin of 3-5% is adequate for square and rectangular column forms designed to withstand the loading conditions mentioned above. **(Korentz, 2020)** conducted a numerical study on the effect of three dominant parameters on the buckling capacity and postcritical response of reinforcing bars in RC columns. These were the initial shape of deformation, the amplitude of geometric imperfection, and the slenderness ratio of bars. All three factors have a significant impact on inelastic buckling behavior. Note that the buckling resistance of bars with initial curvature or compressive deformation was lower than that of straight bars, particularly at higher imperfection amplitude and slenderness.

Fiber-reinforced polymer (FRP) composites are now widely used in civil engineering applications due to their excellent performance-to-weight ratio, including strength-to-weight ratio, stiffness-to-weight ratio, durability, and corrosion resistance **(Mahboubi and Shiravand, 2019; Shaikh and Alishahi, 2019; Naqe and Al-zuhairi, 2020; Yan et al., 2021)**. These materials, commonly produced in sheets, strips, or fabrics, can be used as rehabilitative techniques for RC structures. With its lightweight, high tensile strength, low-cost installation, and capability of rapid return to service, as well as a return to or, in some cases, even an increase over the original level of structural capacity, FRP strengthening has been widely used to enhance RC columns and improve column performance since the mid-1980s **(Van Cao and Pham, 2019; Ayazian et al., 2021; Samy et al., 2022)**. Furthermore, the use of FRP sheets to strengthen RC columns, particularly in substandard buildings and bridges, is widespread. **(Al-Nimry and Al-Rabadi, 2019)**.

Based on fiber type, FRPs can be categorized as carbon (CFRP), glass (GFRP), basalt (BFRP), and aramid (AFRP) fiber-reinforced polymers **(Sadeghian and Fillmore, 2018; Tafsirojjaman et al., 2022)**. Of these, CFRP is the most commonly used and well-investigated technique. CFRP has been widely used as reinforcement for structures, including reinforced concrete columns, due to its high strength-to-weight ratio, excellent corrosion resistance, ease of installation, and customizable properties **(Castro Quispe et al., 2024)**. Experimental investigations have demonstrated that CFRP can significantly enhance the cracking resistance and ultimate load capacity of reinforced concrete (RC) components **(Al-Ahmed and Al-Jburi, 2016)**. CFRP confinement can enhance the load capacity of both axially and eccentrically loaded columns **(Abokwiek et al., 2021)**. Additionally, the confinement of compression members with CFRP jackets proved highly successful, with load-carrying capacity enhancements exceeding 56% for confined specimens compared to unconfined ones, as reported in some studies **(Abdulsattar and Al-Baghdadi, 2020)**.

Many studies have been conducted to research the behavior of concrete columns jacketed with CFRP under various loading conditions and for a wide range of axial and lateral performance. Nevertheless, an initial presence of geometric imperfections in the structural models was not explicitly included in most of these studies.

For short RC columns, **(Mai et al., 2018)** analyzed the performance of square RC columns confined separately with full and partial CFRP wraps, and their results indicated that CFRP

confinement, either complete or incomplete, had a significant enhancement impact on both the strength and ductility of RC square columns. Although **(Mercimek et al., 2020)** did not use complete jacketing, this study was selected because the CFRP confinement of RC-deficient square columns indicates that the CFRP-strengthened columns increased the axial load capacity of the tested columns by 53% and their initial stiffness by about 70%.

For slender RC columns, a study by **(Saleh et al., 2022)** has shown that CFRP can confine slender RC columns while simultaneously increasing their compressive strength and ductility. Nevertheless, the literature has shown that the effectiveness of CFRP confinement decreases substantially for slender columns compared to short columns **(Saleh et al., 2022)**. Furthermore, **(Narule and Bambole, 2021)** studied the axial response of slender RC rectangular columns of varying sizes strengthened with CFRP, subjected to different slenderness ratios. The experimental results showed that the slenderness ratio significantly affects the ultimate strength, yield strength, and ductility of the CFRP-wrapped RC columns. Additionally, **(Ali et al., 2023)** conducted an experimental study on the structural behavior of slender recycled aggregate concrete (RAC) columns wrapped with CFRP jackets, and their test results indicated that either the type of lateral reinforcement or the quantity of CFRP wrapping had a significant effect on the loading capacity of the columns.

Although numerous experimental studies have investigated CFRP strengthening of RC columns, most have primarily focused on strength enhancement and ductility improvement. In many of these studies, the columns were assumed to be initially straight, and the influence of initial geometric imperfections was not explicitly considered. In addition, CFRP confinement has commonly been investigated for columns with adequate transverse reinforcement, while the behavior of columns with inadequate interior ties has received comparatively limited attention. Consequently, the combined influence of initial geometric imperfections, inadequate interior ties, and CFRP confinement remains insufficiently investigated, particularly in numerical studies used to evaluate agreement with design code provisions. **(ACI PRC 318, 2025; ACI PRC 440.2, 2023)** provide detailed design provisions for unconfined and confined RC columns, respectively. However, these codes do not explicitly specify limits for initial geometric imperfections in RC columns, such as an initial out-of-straightness (e.g., $L/1000$), where L represents the unsupported length of the column, ℓ_u. Consequently, this study employs detailed finite element analysis (FEA) using Abaqus/CAE to investigate the influence of initial geometric imperfections on the structural response of RC columns.

Initially, the study examines the impact of explicitly accounting for initial geometric imperfections in the FEA, including both global and local imperfections, on the load-carrying capacity and ductility of RC columns. Second, the study investigates the significance of these imperfections on the behavior of RC columns. Third, the study evaluates the effect of initial geometric imperfections on confined and unconfined square RC columns strengthened with CFRP jacketing. Accordingly, both global and local initial imperfections were explicitly incorporated into the numerical models. The resulting numerical predictions were then compared with the axial capacity predictions prescribed by **(ACI 318, 2025; ACI PRC 440.2, 2023)**. These results were further used to perform a code-based calibration of the Abaqus finite element (FE) models.

Furthermore, a code-based numerical study was conducted to assess the behavior of short and slender square RC columns with inadequate interior ties when initial geometric imperfections are considered, by comparing the numerical predictions with ACI-based requirements for CFRP-jacketed cases with and without interior ties.

2. COLUMN GEOMETRY AND CONFIGURATIONS

The study problem was addressed by using short, slender square reinforced concrete (RC) columns with a constant cross-sectional size of 560 × 560 mm. The short columns were 3,000 mm high, and the slender ones were 7,000 mm high. As shown in **Fig. 1**, Columns A and B were designed using the same geometry (and boundary condition) but with adequate and inadequate interior ties. For the column configurations, a labeling system has been used to clearly distinguish between these different enhancements, where each suffix of "A" or "B" represents the particular reinforcement arrangement within that column.

Slenderness effects may be neglected in braced and unbraced systems, depending on the member's slenderness ratio ($k\ell_u/r$). Hence, the slenderness ratio according to ACI 318-25 provisions for columns braced against sideways is calculated as follows **(ACI Committee 318, 2025)**.

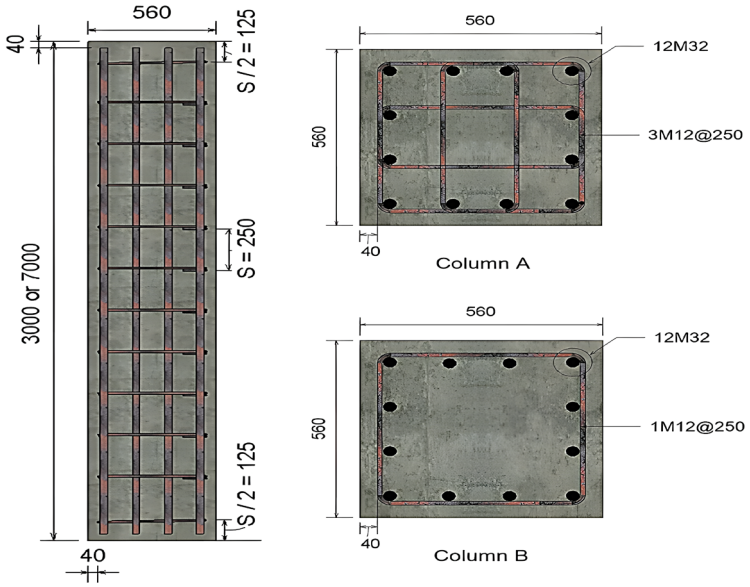

Figure 1. Geometric details of the square RC columns (all dimensions are in mm).

where r is the radius of gyration equal to 0.3 times the column height ($0.3h$) in rectangular columns, k is the effective length factor that equals 1.0 for columns with pin-ended supports **(Darwin and Dolan, 2021)**. The columns shown in **Fig. 1** were classified based on their slenderness ratio. The 3 m columns were identified as short columns, with a slenderness ratio of 18, whereas the 7 m columns were classified as slender columns, with a slenderness ratio of 42.

To achieve optimal confinement effectiveness in CFRP-confined columns, the edges of the concrete cross-section were rounded to a corner radius (r_c) of 25 mm in this study, which was used to construct the interaction diagram and to model the FE, as shown in **Fig. 2**.

This study examines full-scale RC columns derived from finite element (FE) models. A consistent and clear labeling system was used between different configurations and modeling types. It is a three-capital-letter label plus a suffix. The initial letter signifies the slenderness of the column: S for short columns and L for long (slender) ones. The second letter represents confinement conditions: U of unconfined columns, C of CFRP confined columns. The third letter (for example, A or B) indicates differences in reinforcement details only between Column A and Column B, as previously shown in **Fig. 1**.

Numerical (full-scale FE) models are indicated with a suffix "-F". Every numerical model was produced in a separate configuration. For instance, SUA-F is the full-scale numerical model of a short, unconfined Type A column.

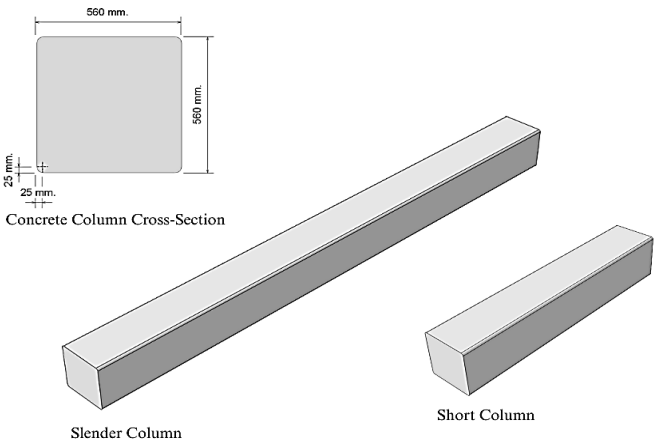

Figure 2. Concrete parts for square short and slender RC column models with a r_c equal to 25 mm in Abaqus/CAE.

3. ACI INTERACTION DIAGRAM

An interaction diagram shown in **Fig. 3** was created in accordance with the strain compatibility procedure prescribed by **(ACI PRC 318, 2025; ACI PRC 440.2, 2023)** for Column A.

Fig. 3 shows four points (A, A′, B, and C) selected to calculate P_n, M_n, and e for both unconfined and confined columns. These points were used to construct the axial load–bending moment interaction diagram for Column A with the cross-section shown in **Fig. 1**.

In this study, six plies of CFRP wrap were used to strengthen the column. Six CFRP plies were adopted as a practical strengthening level for full-scale RC columns without introducing excessive confinement. This strengthening is achieved with a CFRP volumetric ratio of approximately 0.7%, which provides sufficient lateral confinement while compensating for the absence of interior ties.

Point A was calculated using the nominal axial-load equation at zero eccentricity for the unconfined and confined columns, respectively, with the neutral-axis depth (c) assumed to be infinite.

Point A′ was taken as accidental eccentricities (α) times the nominal axial load at Point A, where α equals 0.8 for columns with ties as transverse reinforcement according to ACI 318-25. P_n, M_n, and e at Point B were calculated using a neutral axis depth (c) of 492 mm for both the confined and unconfined columns. For Point C, the neutral axis depth at balanced failure (c_b) was calculated as 289 mm for the unconfined column and 335 mm for the confined column. For both Points B and C, the ultimate concrete compressive strain (ε_u) of 0.003 for the unconfined column and the ultimate compressive strain of confined concrete (ε_{ccu}) of 0.0041 were determined according to the adopted ACI code-based formulations.

The interaction diagram was established using the same material properties used in numerical modeling, including concrete, reinforcing steel, and CFR.

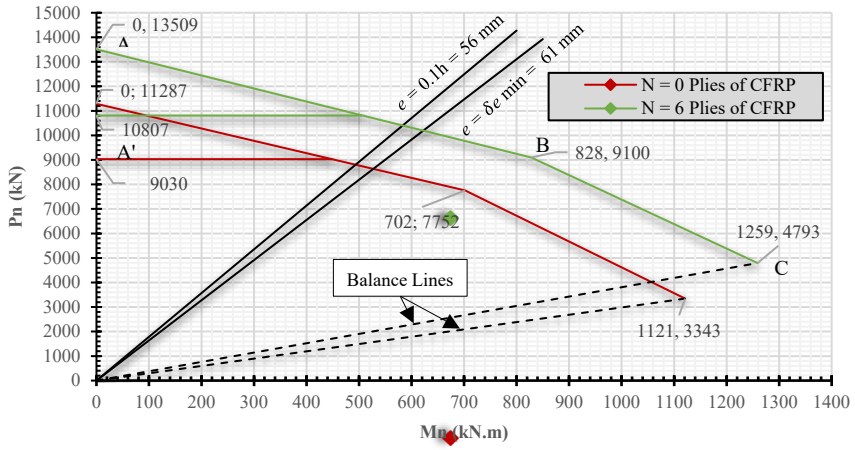

Figure 3. Interaction diagram for columns based on ACI code equations.

This diagram served as a reference for assessing code-based calibration axial capacity and comparing FEA results in two cases, with and without wrapped CFRP, where P_n is the nominal axial load, M_n is the nominal flexural strength, e is the load eccentricity of the column, and δ is the moment magnification factor, as defined in **(ACI Committee 318, 2025)**. The notation for the number of CFRP plies (N) follows the provisions of **(ACI Committee 440, 2023)**.

The constructed interaction diagram, shown in **Fig. 3**, indicates that at Point A corresponding to zero eccentricity, P_n the short column was 11,287 kN for the unconfined condition. In contrast, it increased to 13,509 kN for the confined column strengthened with six CFRP plies.

Furthermore, for the slender column at the minimum eccentricity (δe_{min} = 61 mm), P_n and M_n for the unconfined column are 8640 kN and 527 kN·m, respectively. In contrast, for the column strengthened with six CFRP plies, P_n and M_n are 10,200 kN and 622 kN·m, respectively. Therefore, using six plies of CFRP increases the strength of the slender column (7 m in height), corresponding to an 18% enhancement due to CFRP confinement.

4. ABAQUS FINITE ELEMENT MODELING

4.1 Element Types

The RC columns are modeled as solid (continuum) elements with a square cross-section, and truss elements are used to simulate the longitudinal reinforcement bars as wire parts. Shell elements are used to simulate the CFRP sheets.

4.2 Material Modeling

4.2.1 Concrete Modeling

The compressive strength of concrete (f_c') would be 28 MPa, which is a typical value for structural design.

In this study, Abaqus/CAE is used for FEA. The concrete damaged plasticity (CDP) model can be used. When the concrete-damaged plasticity model in Abaqus/CAE is used, it yields good agreement between experimental and numerical results **(Kadhim et al., 2025)**. The concrete behavior was modeled using the CDP model in Abaqus, which captures the nonlinear response of concrete under both compression and tension, including cracking,

crushing, and stiffness degradation **(Lubliner et al., 1989; Lee and Fenves, 1998)**. The CDP parameters adopted in the numerical models are shown in **Table 1**, as reported by **(Hafezolghorani et al., 2017)**.
For concrete, the Young's modulus was taken as 24,870 MPa, Poisson's ratio was 0.20, and the modulus of rupture was 3.3 MPa, in accordance with ACI 318-25. Additionally, the tensile cracking strain used in the CDP model in this study was defined based on the stress–strain relationship proposed by **(Hafezolghorani et al., 2017)**.

Table 1. CDP parameters adopted in the numerical models **(Hafezolghorani et al., 2017)**.

Dilation angle	Eccentricity	Ratio of biaxial to uniaxial compressive strength ($fb0/fc0$)	Shape factor of the yield surface (K)	Viscosity parameter
37	0.01	1.16	0.667	0

4.2.2 Steel Reinforcement Modeling

Longitudinal and transverse steel reinforcement was used with a yield strength (f_y) of 420 MPa, which is commonly used for Grade 60 bars in RC design and is consistent with the requirements of **(ACI Committee 318, 2025)**. The Young's modulus was 200000 MPa, and Poisson's ratio was 0.3.

4.2.3 CFRP Modeling

The CFRP material was modeled as a linear elastic orthotropic fiber-reinforced composite, using the mechanical properties listed in **Table 2**. These properties are in accordance with the material data adopted by **(Sudhir Sastry et al., 2014; Fosroc, 2019)**.

Table 2. Mechanical properties of the CFRP plies **(Sudhir Sastry et al., 2014; Fosroc, 2019)**.

Product grade	Nitowrap CWS
Fiber density (g/cm3)	1.8
Fiber area weight (g/m2)	300
Standard roll width (mm)	500
Standard roll length (m)	100
Design thickness (mm)	0.166
Ultimate elongation or rupture strain	2.1%
Fiber E-modulus at 0° (MPa)	230×103
Fiber E-modulus at 90° (MPa)	12000
Longitudinal Tensile strength (MPa)	3481
Transverse Tensile strength (MPa)	50
Shear modulus in planes 12 and 13 (MPa)	4500
Shear modulus in plane 23 (MPa)	2500
Poisson's ratio in planes 12 and 13	0.32
Poisson's ratio in planes 23	0.45

4.3 Material Interaction Modeling and Mesh Size

An Abaqus embedded region constraint has been used to model a perfect bond between the concrete and the rebar. A tie constraint has been used between the concrete and CFRP. A

mesh size of 40 mm was adopted for the concrete elements of the full-scale RC column to ensure geometric compatibility and to represent the 40 mm concrete cover properly. In comparison, a finer mesh size of 20 mm was used for the CFRP jackets. The selected mesh sizes were considered sufficient to capture the global response of the CFRP-strengthened RC column while maintaining reasonable computational efficiency.

A convergence study was conducted on a representative column model (SCB-F) using coarser and finer meshes to justify the selected final mesh. The estimated final (maximum) axial loads for the coarse, medium, and fine meshes were 12,283 kN, 12,493 kN, and 12,495 kN, respectively, with associated axial displacements at the maximum load of 7.1 mm, 9.9 mm, and 10.0 mm, respectively. The difference between meshes was less than 1% for both load and displacement, indicating that mesh convergence was achieved. Hence, the adopted mesh (40 mm for concrete and steel, and 20 mm for CFRP) was used in all subsequent analyses. Since the CFRP layer is very thin and transmits confinement stresses into the concrete core, a finer mesh was applied for the CFRP jacket. The refinement enhances the accuracy of stress transfer and interaction at the CFRP–concrete interface.

4.4 Boundary Conditions and Loading

A uniform compressive stress of 60 MPa was applied to the top surface of the square RC column models. This value was deliberately chosen to exceed the expected capacity, so that the nonlinear incremental analysis can be allowed to reach failure. The columns were modeled with pinned boundary conditions at both the upper and lower ends. The pinned–pinned boundary condition was used to model columns in braced frames, where the lateral translation of a joint is restricted. Column ends in practice are rarely purely hinged or fixed and will almost always have partial rotational restraint **(Darwin and Dolan, 2021)**. As a result, an effective length factor (k) of approximately 1.0 was adopted in the numerical model for slenderness evaluation, in accordance with ACI recommendations **(Hassoun and Al-Manaseer, 2020)**.

Furthermore, the structure's self-weight was not accounted for to maintain consistency with the analytical solution's assumptions. The self-weight (concrete and longitudinal reinforcement) was neglected, as it accounts for only approximately 0.5–1% of the axial load based on the column dimensions and material unit weights for the studied, with heights of 3 m and 7 m. Hence, no significant impact on the nonlinear response and stability behavior.

5. COMPARISON OF ELASTOPLASTIC STRENGTH ANALYSIS PREDICTIONS WITH ACI CODE

In this study, an FEA of the column models was conducted for strength analysis, and the results were obtained. The main objective of this study is to develop axial load–axial displacement (P–Δ) curves for both column types, providing a clear indication of their behavior under different slenderness ratios and with and without interior ties, with and without six plies of CFRP applied. It should be noted that geometric nonlinearity was activated in the FEA by enabling the NLGEOM option to account for significant displacement effects and stability-related behavior.

The strength analyses (P–Δ) performed in Abaqus/CAE for all models of short and slender columns are summarized in **Table 3**. The table was organized to systematically present the numerical analyses conducted in this study, along with the differences in P_n compared with the previously obtained values from the constructed interaction diagrams presented in

Section 3, where unconfined columns were compared with (**ACI 318, 2025**), and confined columns with six layers of CFRP were compared with (**ACI PRC-440.2, 2023**).

Table 3. FEA results (P–Δ response) for short and slender square RC columns, and comparison of P_n obtained from FEA with ACI 318-25 and ACI PRC-440.2-23 predictions.

RC Short Columns					RC Long Columns				
Column Name	ACI Code	FEA			Column Name	ACI Code	FEA		
	P_n (kN)	P_n (kN)	Δ (mm)	Diff. (%)		P_n (kN)	P_n (kN)	Δ (mm)	Diff. (%)
SUA-F	11287	12099	6.4	7	LUA-F	8640	12099	14.0	40
SCA-F	13509	13208	7.4	2	LCA-F	10200	13208	16.0	29
SUB-F	11287	10880	5.3	4	LUB-F	8640	10881	11.4	26
SCB-F	13509	12493	9.9	8	LCB-F	10200	12493	18.2	22

According to the table above for short square RC columns, the difference in column strength, SUA-F, compared to the **(ACI PRC 318, 2025)** prediction is approximately 7%. In contrast, the difference between the SCA-F and the **(ACI PRC-440.2, 2023)** provisions is roughly 2%. These differences indicate satisfactory agreement, meaning that the computed results for the short square RC columns are acceptable and comparable. The P_n decreased from 12,099 kN in the SUA-F to 10,880 kN in the SUB-F, representing a reduction of about 10%. However, this reduction in strength was effectively compensated for by using six CFRP plies in the SCB-F model, resulting in a 3% difference in strength between SUA-F and SCB-F, with SCB-F showing an increase of approximately 394 kN. These results suggest that the absence of interior ties led to a lower P_n; however, the CFRP jacket's confinement action effectively compensated for this.

In both short and slender square RC columns, Δ was improved by the use of CFRP. The difference between SUA-F and SCA-F was approximately 16%, whereas it showed a 14% difference between their corresponding slender columns (LUA-F and LCA-F). In comparison, the Δ decreased when no interior ties were present. The difference between SUA-F and SUB-F was 17%, and between LUA-F and LUB-F was 19%. Furthermore, the P–Δ Curves for short square RC column models are presented in **Fig. 4**. The results show that the strength and ductility were still improved in the SCA-F compared with the SUA-F, whereas the SUB-F showed an apparent decrease in both values. The SCB-F model has demonstrated that CFRP jackets, composed of six layers, adequately replace the absence of interior ties in SUB-F, as evidenced by an increase in strength and ductility greater than that found in the unstrengthened SUA-F model. According to ACI PRC-440.2-23, the concrete's ability to withstand higher levels of compressive strain before failure is a primary contributor to enhanced section ductility. It is also evident from **Fig. 4** that both strength and ductility decrease with the absence of interior ties in SUB-F and SCB-F.

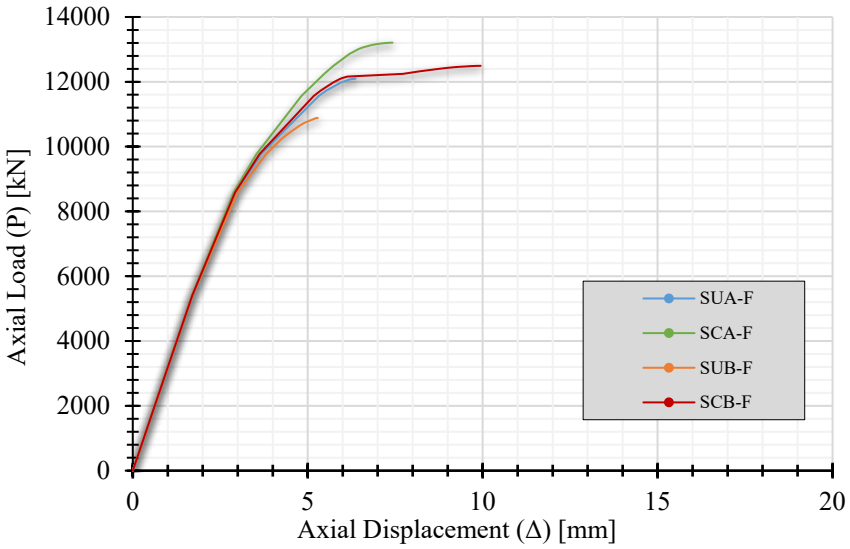

Figure 4. *P–Δ* curves of short square RC columns obtained from strength analysis using Abaqus/CAE.

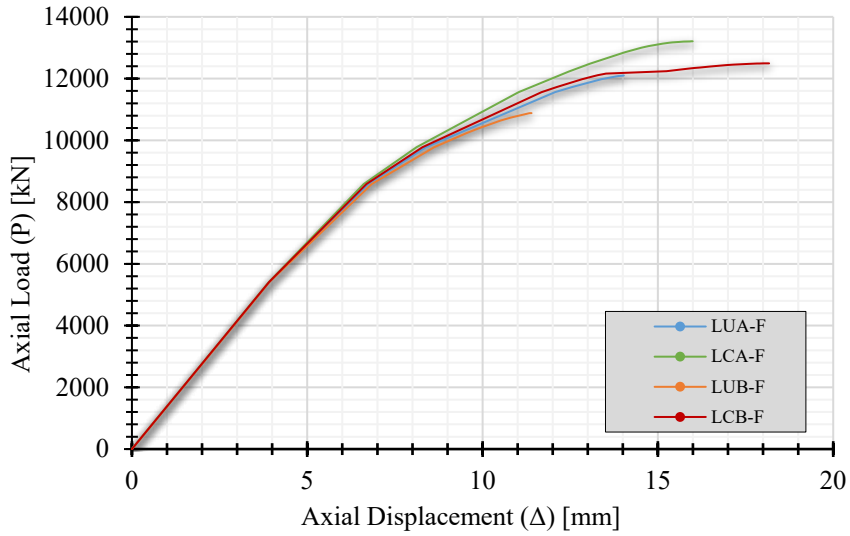

Figure 5. *P–Δ* curves of slender square RC columns obtained from strength analysis using Abaqus/CAE.

For slender square RC columns, **Table 3** shows an inconsistency between the numerical findings and those calculations from ACI 318-25 and ACI PRC-440.2-23. The P_n of the slender columns is very similar to that of the short columns shown in **Fig. 5**. These results indicate that the slenderness effects associated with buckling behavior were not sufficiently represented in the initial Abaqus/CAE simulations. Although an increase in *Δ* was observed, indicating a partial consideration of second-order effects, no significant change was noted in P_n. These observations highlight the need to introduce appropriate modeling strategies, such as initial geometric imperfections, to enable Abaqus/CAE to adequately capture slenderness effects in the structural strength analysis of slender RC columns.

6. INITIAL GEOMETRIC IMPERFECTIONS IN RC COLUMNS

Initial geometric imperfections are commonly introduced in structural analysis to represent worst-case fabrication and erection tolerances and to capture the most critical stability response. According to **(AISC 360, 2022)**, Although not mandatory for all structural systems, an initial out-of-straightness of $L/1000$ is still considered a representative magnitude of geometric imperfections and is widely adopted in stability-related analyses. As indicated in **(AISC 360, 2022)**, Geometric imperfections can be represented using an amplitude of $L/1000$, which is commonly adopted as a representative value in stability-related design and assessment. As noted in **(Dassault Systèmes, 2025)**. The geometric imperfection scale factor (GISF) can be introduced into the FE model. For instance, a column with a length of 3000 mm, the GISF is 3000/1000, equivalent to an amplitude of 3 mm. However, in this study of short and slender columns, different GISFs were used. In the FEA using Abaqus/CAE, global geometric imperfections were introduced into the RC column models following a two-step procedure. First, a linear buckling stability analysis was performed, and the resulting eigenmode shape was exported, as illustrated in **Fig. 6(a)**. This mode shape was then imported into the subsequent elastoplastic strength analysis as the initial geometry. In the second step, as shown in **Fig. 6(b)**, the imported first buckling mode was scaled to a prescribed amplitude to represent the initial geometric imperfection. This was achieved by applying a GISF corresponding to an amplitude of 3 mm. Accordingly, both steps are required to implement a global geometric imperfection in the numerical model, in accordance with the procedure outlined by **(Dassault Systèmes, 2025)**.
Additionally, local geometric imperfections cannot be generated by a preceding buckling analysis and must be introduced directly at the elastoplastic strength analysis stage.

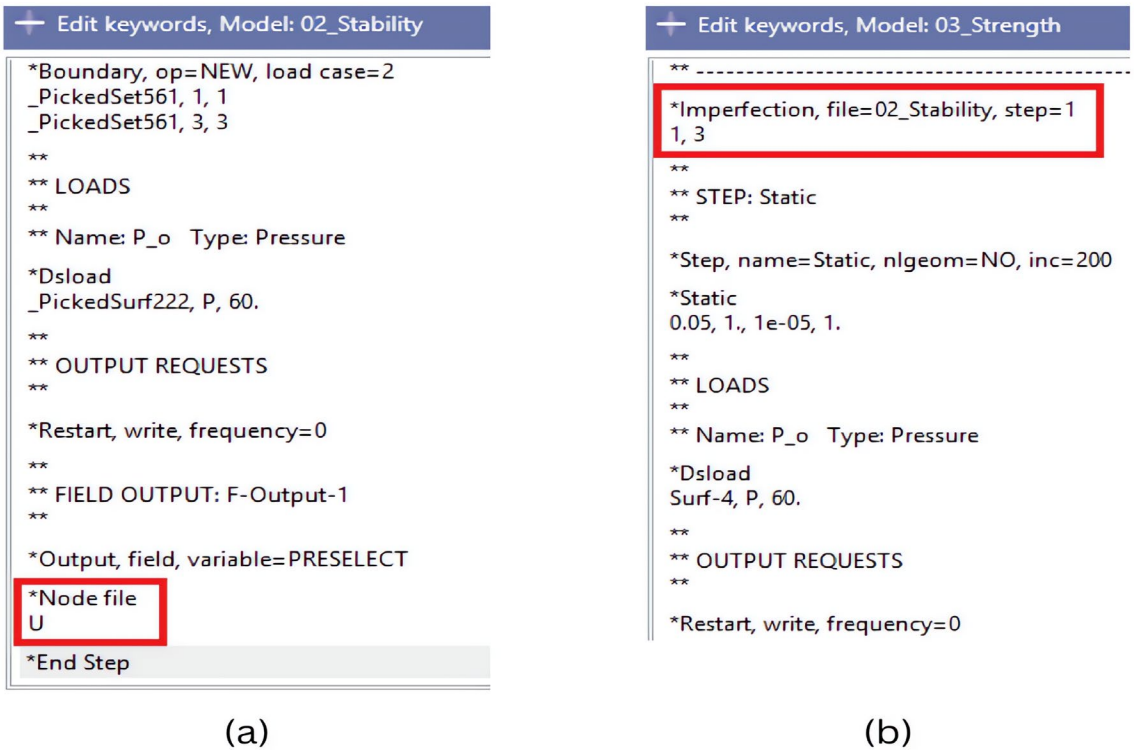

Figure 6. Application of global imperfection in Abaqus/CAE for RC column models using GISF equal to 3 mm.

7. RESULTS AND DISCUSSION

7.1 Influence of the Initial Geometric Imperfections on the Response of Short Square RC Columns

The full-scale short columns (SUA-F and SUB-F) were modeled in FEA using Abaqus/CAE. In the first scenario, an initial global imperfection is applied; in the second scenario, a local rebar imperfection is applied.

7.1.1 Global Imperfection Scenario for Short Square RC Columns

The summary of the P–Δ results for model short columns (SUA-F and SUB-F) under different GISFs are shown in **Table 4**. The table also compares the P_n of SUA-F obtained by FEA with that predicted by **(ACI Committee 318, 2025)**. Furthermore, it compares the P_n of SUA-F and SUB-F to assess the impact of interior ties.

Table 4. Summary of P–Δ results for short square RC column models showing differences of P_n for SUA-F and ACI 318-25, and SUA-F and SUB-F under different GISF amplitudes.

	(ACI PRC 318, 2025)	FEA					
		SUA-F			SUB-F		
GISF	**P_n (kN)**	**P_n (kN)**	**Δ (mm)**	**Difference with ACI 318 Code (%)**	**P_n (kN)**	**Δ (mm)**	**Difference with SUA-F (%)**
without	11287	12099	6.4	7	10880	5.3	10
$L/1000$	—	12000	6.1	6	10876	5.3	9
$L/200$	—	11383	5.6	1	10725	5.2	6
$L/175$	—	11270	5.5	≈ 0	10681	5.1	5

As shown in the table above, when the amplitude of GISF increased, P_n and Δ decreased. When the GISF amplitude of $L/175$ was used, the results were in close agreement with **(ACI PRC 318, 2025)**, with no significant differences. Moreover, the difference in P_n between SUA-F and SUB-F was 10% when no imperfection was added initially. On the other hand, this difference decreased to 5% when using GISF equal to $L/175$, and the axial displacement also decreased for short columns in FEA, highlighting the significant effect of buckling behavior on RC columns if a global imperfection scenario is applied in FEA.

Fig. 7 shows the deformed shape of a representative column (both SUA-F and SUB-F) with pinned support in the FEA model after global imperfection was imposed. It illustrates both three-dimensional (3D) and side views. A single representative column is shown because the deformed shape of SUA-F resembled that of SUB-F.

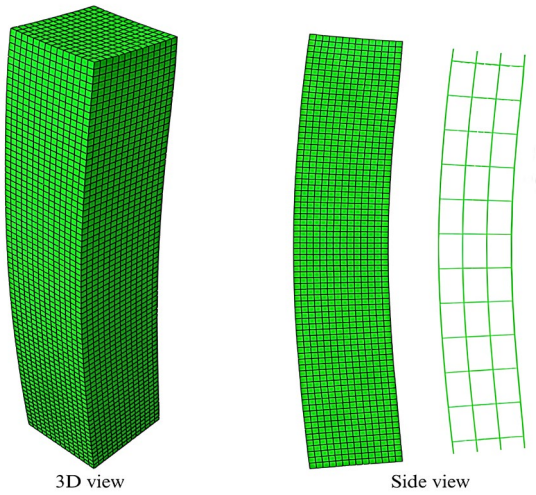

Figure 7. Deformed shape of the representative column model (SUA-F and SUB-F) with pinned support and global imperfection, shown in 3D and side views.

7.1.2 Short Square RC Columns with Local Imperfection of Rebars Scenario

In the strength FEA, various amplitudes of GISFs were considered based on a tie spacing (s) of 250 mm for this analysis. The longitudinal bars were simulated with local imperfections in SUA-F and SUB-F (see **Fig. 8**).

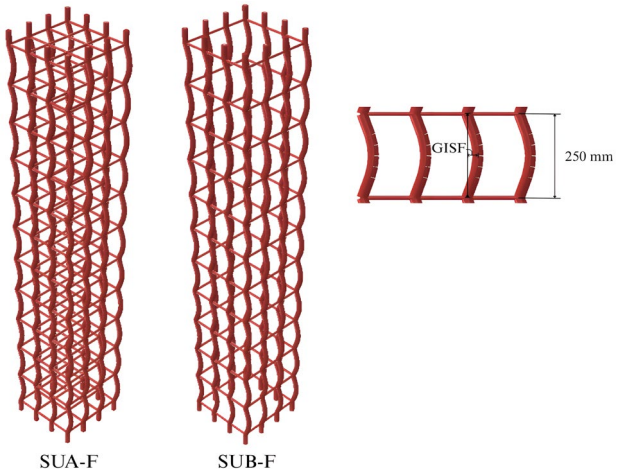

Figure 8. Modeling of Longitudinal Reinforcing Bars in SUA-F and SUB-F with local imperfection introduced with different GISF amplitudes in Abaqus/CAE.

The differences in P_n relative to ACI 318-25 and concerning SUB-F for all results of the $P–\Delta$ response for SUA-F and SUB-F with rebar local imperfections are summarized in **Table 5**. The table shows that the axial load decreases as the GISF amplitude increases. However, it does not significantly affect the axial displacement values. Additionally, it suggests that the impact of rebar imperfection on its strength is minimal, with a slight influence on ductility.

Table 5. *P–Δ* results for SUA-F and SUB-F with local imperfection of rebars, their differences from the ACI 318-25, and between each other.

	ACI PRC 318, 2025)	FEA					
		SUA-F			SUB-F		
GISF	P_n (kN)	P_n (kN)	Δ (mm)	Difference with ACI 318 Code (%)	P_n (kN)	Δ (mm)	Difference with SUA-F (%)
without	11287	12099	6.4	7	10880	5.3	10
$s/1000$	—	12098	6.4	7	10880	5.3	10
$s/250$	—	12079	6.3	7	10874	5.3	10
$s/100$	—	12006	6.3	6	10833	5.3	10

Moreover, a more pronounced imperfection effect is observed in the SUB-F model with inadequate interior ties than in the global imperfection scenario, in which the impact of insufficient interior ties becomes increasingly pronounced as the GISF increases. In addition, the difference in P_n between SUA-F and SUB-F is 10%, and the difference in Δ between the same models is 16%. According to these results, when no interior ties are provided in the column, both strength and ductility decrease. According to FEA, without applied initial geometric imperfections, the P_n for the SCA-F model was 13,208 kN, while for the SCB-F model, it was 12,493 kN, as previously shown in **Table 3**. Additionally, the P_n obtained from the constructed interaction diagram for the RC column strengthened with six CFRP plies was 13,509 kN.

The difference in P_n between ACI 318-25 and SUA-F was approximately 7%, whereas the difference in P_n between ACI PRC-440.2-23 and SCA-F was about 2%. These results indicate that, for the short square RC columns strengthened with CFRP jackets considered in this study, the numerical predictions are in close agreement with ACI PRC-440.2-23. Accordingly, the influence of initial geometric imperfections on the predicted capacity appears negligible for these cases. It is essential to note that these comparisons in this study were conducted using both ACI 318-25 and ACI PRC-440.2-23, focusing on P_n values, while neglecting the strength reduction factor (ϕ) and accidental eccentricities (α) that are used according to these provisions. However, ACI 318-25 and ACI PRC-440.2-23 would make even more conservative predictions than FEA models (with initial geometric imperfections) when considering the factors ϕ, α, or both.

Although ACI 318-25 and ACI PRC-440.2-23 do not explicitly use the term "Initial geometric Imperfections," their effects are implicitly incorporated through the consideration of accidental eccentricities applied to the nominal axial load (αP_n). As noted by **(Darwin and Dolan, 2021)**, The ACI Code requires accidental eccentricities to be added to the design strength of RC columns to account for additional loading effects that are not directly captured in analysis. In this context, the inclusion of accidental eccentricities may be interpreted as a conservative design measure, whereby the ACI provisions implicitly account for the effects of initial geometric imperfections in short RC column design.

7.2 Influence of the Initial Geometric Imperfections on the Response of Slender Square RC Columns

FE models of the slender columns (LUA-F and LUB-F) with various GISF amplitudes were created to examine their performance in both global and local imperfection scenarios, and the results were then compared with those of ACI 318-25 and ACI PRC-440.2-23.

7.2.1 First Scenario of Global Imperfection in Slender Square RC Columns

The FEA for this scenario, involving columns with global initial geometric imperfections and pinned boundary conditions at both ends, is similar to that previously adopted for short square RC columns.

The eccentricity (e) of the axially loaded slender column, which was calculated according to ACI 318-25 in the constructed interaction diagram, where δe_{min} equals 61 mm, is adopted as the GISF amplitude, where e_{min} is the minimum eccentricity for slender RC columns, as shown below, Eq (1).

$$Geomatric\ Imperfection\ Scaleing\ Factor\ (GISF) = \frac{L}{L/e} = e = \delta e_{min}\ (mm) \quad (1)$$

Thus, the GISF is equal to 61 mm.

Table 6 summarizes the $P–\Delta$ results obtained from FEA of model slender columns (LUA-F and LUB-F) at different GISF amplitudes. The table also presents the P_n of LUA-F computed by FEA and compares it with the ACI 318-25 prediction. In addition, it presents a comparison of the P_n values between LUA-F and LUB-F. As shown in **Table 6**, increasing the GISF decreases the $P–\Delta$ results of slender columns, indicating less strength and ductility. Also, when a GISF of δe_{min} is used, LUA-F produces the closest conservative value of P_n compared to ACI 318-25, resulting in a difference of approximately 4%.

Table 6. $P–\Delta$ results in slender columns subjected to the global imperfection of the first scenario, comparing between LUA-F and ACI 318-25, and between LUA-F and LUB-F.

	ACI PRC 318, 2025)	FEA					
		LUA-F			LUB-F		
GISF	P_n (kN)	P_n (kN)	Δ (mm)	Difference with ACI 318 Code (%)	P_n (kN)	Δ (mm)	Difference with LUA-F (%)
without	8640	12099	14.0	40	10881	11.4	10
$L/1000$	—	11181	11.5	29	10850	11.6	3
$L/200$	—	9422	9.4	9	9206	9.2	2
$L/150$	—	8887	9.2	3	8681	8.8	2
δe_{min}	—	8321	9.0	4	8124	8.6	2
$L/\delta e_{min}$	—	6592	8.6	24	6451	8.2	2

The difference in P_n between LUA-F and LUB-F decreases from 10% without imperfection to about 2%. It is also observed that the difference in Δ, which is 23% without imperfection, reduces to 4% when the magnitude of the initial geometric imperfection is limited to an amplitude equal to δe_{min}. This behavior is primarily attributed to the adoption of linear buckling stability analysis to define the initial geometric imperfections. Since the imposed imperfection is based on the first global buckling mode, the response of the slender square RC columns becomes governed mainly by buckling behavior. Consequently, the influence and sensitivity of interior ties, which primarily affect material confinement, are significantly reduced in the presence of such global imperfection patterns.

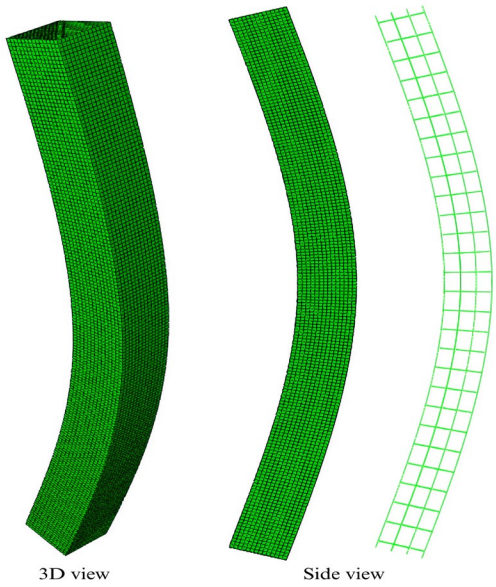

Figure 9. Deformed shape of the representative column model (LUA-F and LUB-F) with pinned supports and global imperfection, shown in 3D and side views.

The deformed shape of a representative slender square RC column model is shown in **Fig. 9**, as LUA-F and LUB-F exhibited nearly identical deformation behavior when a global imperfection was applied using GISF equal to δe_{min}. The FEA was performed using Abaqus/CAE by applying GISF equal to δe_{min} to assess the behavior of LCA-F and LCB-F models and compare their performance with the provisions of ACI PRC-440.2-23. Accordingly, $P–\Delta$ curves for these columns with global imperfection are illustrated in **Fig. 10**, which establishes a suitable initial study for the investigation of axial load-axial displacement response and the effect of using CFRP jacketing to strengthen slender square RC columns. According to **Fig. 10**, the P_n of LCA-F is 9065 kN, while the P_n obtained from the constructed interaction diagram for the same slender square RC column, according to ACI PRC-440.2-23, is 10,200 kN. These results correspond to a difference in P_n of about 11%, indicating that the FE results are close to the code and remain conservative when considering P_n alone. Furthermore, LCA-F exhibits higher ductility than the other slender columns. Additionally, the P_n for LCB-F is 8773 kN, which is 3% lower than that of LCA-F. These results also highlight that the presence of global imperfection reduces the influence of inadequate interior ties in the LCB-F model.

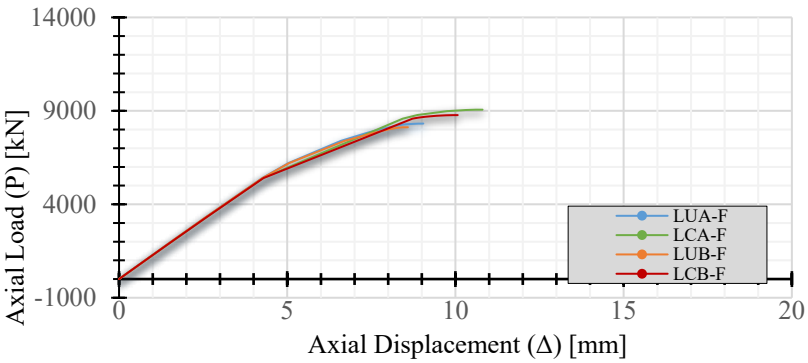

Figure 10. $P–\Delta$ curves for slender square RC column models in the first scenario of global imperfection by applying GISF equal to δe_{min}.

7.2.2 Second Scenario of Global Imperfection in Square RC Columns

The problem of determining the critical buckling load of an elastic column is a key issue in engineering design **(Ibrahim, 2017)**. Given that the slender columns are highly susceptible to buckling, as demonstrated in the first scenario with global imperfection, an additional scenario with global imperfection was considered. In this scenario, the slender column model was assumed to be laterally displaced at one end relative to the other. **Table 7** summarizes the results of the $P-\Delta$ analysis for this scenario, comparing the LUA-F model with ACI 318-25 results and the differences between LUA-F and LUB-F.

Table 7. $P-\Delta$ results in slender columns subjected to the global imperfection of the second scenario, comparing between LUA-F and ACI 318-25, and between LUA-F and LUB-F.

	ACI PRC 318, 2025)	**FEA**					
		LUA-F			**LUB-F**		
GISF	P_n **(kN)**	P_n **(kN)**	Δ **(mm)**	**Difference with ACI 318 Code (%)**	P_n **(kN)**	Δ **(mm)**	**Difference with LUA-F (%)**
without	8640	12099	14.0	40	10881	11.4	10
$L/1000$	—	11448	12.1	33	10877	11.5	5
$L/200$	—	9918	10.0	15	9676	9.7	2
$L/150$	—	9433	9.8	9	9183	9.3	3
δe_{min}	—	8914	9.6	3	8664	8.9	3
$L/\delta e_{min}$	—	7232	9.5	16	6999	8.2	3

The table above shows that the first global imperfection scenario in slender square RC column models with pinned end supports yields a more critical column response than the second scenario. Thus, the first scenario is a more conservative and reliable approach for slender columns than the second scenario. The first scenario was previously adopted in the FEA of short square RC column models.

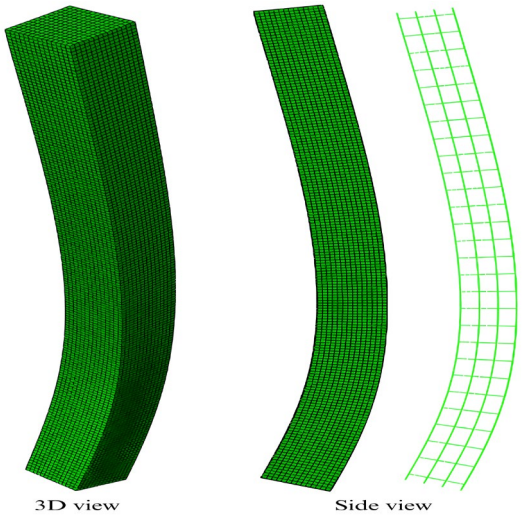

Figure 11. Deformed shape of the representative column model (LUA-F and LUB-F) for the second global imperfection scenario, shown in 3D and side views.

The deformed shape of a representative slender square RC column model with applied global imperfections in the second scenario is shown in **Fig. 11**, as LUA-F and LUB-F exhibited nearly identical deformation behavior when a global imperfection was applied using GISF equal to δe_{min}.

7.2.3 Slender Square RC Columns with Local Imperfection of Rebars Scenario

The same local imperfection of the rebars scenario, as previously used in the short columns, was also applied to the slender columns. A summary of P–Δ results is given in **Table 8**. Longitudinal reinforcing bars in LUA-F and LUB-F were modeled using local imperfections in rebars with GISF amplitudes in the FEA, as shown in **Fig. 12**.

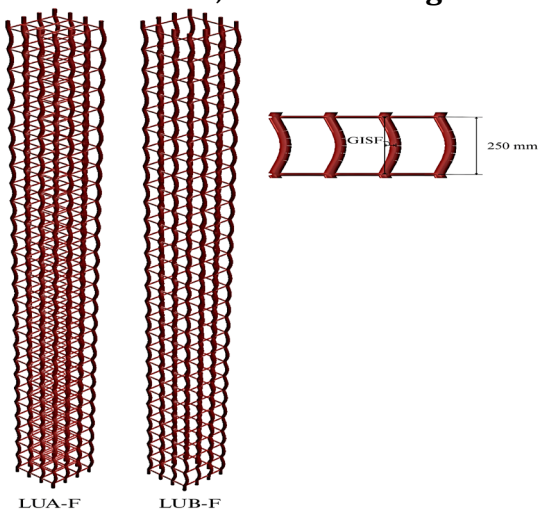

Figure 12. Modeling of Longitudinal Reinforcing Bars in LUA-F and LUB-F with local imperfection introduced with different GISF amplitudes in Abaqus/CAE.

Table 8. P–Δ results for LUA-F and LUB-F with local imperfection of rebars, their differences from the ACI 318-25, and between each other.

	ACI PRC 318, 2025)	FEA					
		LUA-F			LUB-F		
GISF	P_n (kN)	P_n (kN)	Δ (mm)	Difference (%)	P_n (kN)	Δ (mm)	Difference with LUA-F (%)
without	8640	12099	14.0	40	10881	11.4	10
$s/1000$	—	12084	14.0	40	10881	11.4	10
$s/250$	—	12033	13.8	39	10876	11.4	10
$s/100$	—	11860	13.3	37	10831	11.5	9

The table above shows that slender square RC columns behave like short square RC columns when this type of initial imperfection is applied in the FEA. Consequently, the difference in P_n between ACI 318-25 predictions and FEA results will increase, potentially reaching up to 40%. Therefore, the first scenario involving global geometric imperfections is the most consistent with the assumptions adopted in ACI 318-25 and ACI PRC-440.2-23.

To provide a clear overall comparison, **Table 9** summarizes, per case, the initial geometric imperfection scenario that yields the closest agreement between FE predictions and ACI provisions (ACI 318-25 and ACI PRC-440.2-23).

Table 9. Summary of imperfection scenarios providing the closest agreement with ACI provisions.

RC Short Columns					RC Long Columns				
Column Name	ACI Code	FEA			Column Name	ACI Code	FEA		
	P_n (kN)	P_n (kN)	GISF	FE/ACI		P_n (kN)	P_n (kN)	GISF	FE/ACI
SUA-F	11287	11270	$L/175$	1.00	LUA-F	8640	8321	δe_{min}	0.96
SCA-F	13509	13208	No imperfection	0.98	LCA-F	10200	9065	δe_{min}	0.89
SUB-F	11287	10681	$L/175$	0.95	LUB-F	8640	8124	δe_{min}	0.94
SCB-F	13509	12493	No imperfection	0.92	LCB-F	10200	8773	δe_{min}	0.86

As shown in **Table 9**, the first scenario with global imperfections and pinned–pinned column ends provide the closest match. For the SAB model, the FE predictions were already closely in line with results obtained using ACI PRC-440.2-23; thus, the use of geometric imperfections was not necessary. Furthermore, the addition of six CFRP plies compensated for the absence of interior ties in both SCB-F and LCB-F models.

8. CONCLUSIONS

This study investigated the effect of initial geometric imperfections on the reliability of FE models in predicting the behavior of short and slender square reinforced concrete (RC) columns, with and without interior ties, under axial compression. Both confined and unconfined columns strengthened with CFRP jacketing were considered. The primary objective of this research was to evaluate how initial geometric imperfections can be used to achieve a code-based calibration of column models, resulting in P_n predictions in good agreement with the provisions of ACI 318-25 and ACI PRC-440.2-23. The main conclusions of this study are summarized as follows.

- ACI 318-25 and ACI PRC-440.2-23 implicitly account for initial geometric imperfections in RC columns. For short columns this is represented through the inclusion of αP_n, while for slender columns it is considered through δe_{min}.
- For the short square RC columns analyzed in this study, the influence of geometric imperfections on the predicted axial capacity was negligible when the FEA results were in close agreement with the Pn values obtained from ACI 318-25 and ACI PRC-440.2-23 (without applying the ϕ and α factors).
- Increasing the GISF amplitude for global and local imperfections reduces both the strength and ductility of short and slender square RC columns.
- For short square RC columns under global imperfections, employing a GISF amplitude of $L/175$ resulted in negligible differences between the P_n obtained from FEA and that calculated according to ACI 318-25.
- In global imperfection scenarios, the presence of interior ties had a smaller influence on strength and ductility as GISF amplitude increased for both short and slender square RC columns, since the response became governed mainly by buckling behavior.

- The use of adequate CFRP plies in short square RC columns under axial loading conditions without initial geometric imperfections can effectively compensate for the absence of interior ties in terms of strength and ductility.
- Among the investigated cases, the first global imperfection scenario with GISF equal to δe_{min} and pinned-end boundary conditions was identified as the most critical case for slender RC columns and provided the closest agreement with ACI 318-25 and ACI PRC-440.2-23 predictions. In this scenario, the difference in P_n between FEA and ACI 318-25 was approximately 4%, while the difference with ACI PRC-440.2-23 was about 11% when six CFRP plies were used.

Credit Authorship Contribution Statement

Ali Majid Mousa: Methodology, Conceptualization, Software development, Validation, Investigation, Data curation, Writing –original draft, Resources. Salah R. Al Zaidee: Supervision, Writing – review &editing, Guidance on methodology.

Declaration of Competing Interest

The authors declare that they have no known competing financial interests or personal relationships that could have appeared to influence the work reported in this paper.

REFERENCES

Abdulsattar, A.W. and Al-Baghdadi, H.A., 2020. Experimental and numerical study of CFRP-confined square concrete columns under axial compression. *Journal of Engineering*, 26(4), pp. 141–160. https://doi.org/10.31026/j.eng.2020.04.10.

Abokwiek, R., Abdalla, J.A., Hawileh, R.A., and El Maaddawy, T., 2021. RC columns strengthened with NSM-CFRP strips, and CFRP wraps under axial and uniaxial bending: Experimental investigation and capacity models. *Journal of Composites for Construction*, 25(2). https://doi.org/10.1061/(asce)cc.1943-5614.0001117.

ACI PRC 318, 2025. *Building code for structural concrete—Code requirements and commentary (ACI CODE-318-25)*. *318-19 Building Code Requirements for Structural Concrete and Commentary*. Farmington Hills, MI: American Concrete Institute.

ACI PRC 440.2, 2023. *Design and construction of externally bonded fiber-reinforced polymer (FRP) systems for strengthening concrete structures—Guide (ACI PRC-440.2-23)*. Farmington Hills, MI: American Concrete Institute.

Al-Ahmed, A.H.A. and Al-Jburi, M.H.M., 2016. Behavior of reinforced concrete deep beams strengthened with carbon fiber reinforced polymer strips. *Journal of Engineering*, 22(8), pp. 37–53. https://doi.org/10.31026/j.eng.2016.08.03.

Alekseytsev, A.V. and Kurchenko, N.S., 2023. Safety of reinforced concrete columns: Effect of initial imperfections and material deterioration under emergency actions. *Buildings*, 13(4), P. 1054. https://doi.org/10.3390/buildings13041054.

Ali, F.A., Hasan, Q.A. and Mohammed, D.H., 2023. Strengthening of recycled aggregate concrete slender column with CFRP. In: *E3S Web of Conferences*. EDP Sciences. P. 02015. https://doi.org/10.1051/e3sconf/202342702015.

Al-Nimry, H.S. and Al-Rabadi, R.A., 2019. Axial–flexural interaction in FRP-wrapped RC columns. *International Journal of Concrete Structures and Materials*, 13(1). https://doi.org/10.1186/s40069-019-0366-8.

American Institute of Steel Construction, 2022. *Specification for structural steel buildings (ANSI/AISC 360-22)*. 2022nd ed. Chicago, IL.

Ayazian, R., Abdolhosseini, M., Firouzi, A. and Li, C.Q., 2021. Reliability-based optimization of external wrapping of CFRP on reinforced concrete columns considering decayed diffusion. *Engineering Failure Analysis*, 128, P. 105592. https://doi.org/10.1016/j.engfailanal.2021.105592.

Van Cao, V. and Pham, S.Q., 2019. Comparison of CFRP and GFRP wraps on reducing seismic damage of deficient reinforced concrete structures. *International Journal of Civil Engineering*, 17(11), pp. 1667–1681. https://doi.org/10.1007/s40999-019-00429-y.

Castro Quispe, V.J., de Diego Villalón, A., León González, F.J., Martínez de Mingo, S., and Echevarría Giménez, L., 2024. Evaluating the effectiveness of CFRP confinement: New model and simplified estimation of ductility improvement. *Structures*, 70, P. 107825. https://doi.org/10.1016/j.istruc.2024.107825.

Darwin, David. and Dolan, C.W., 2021. *Design of concrete structures*. 16th ed. McGraw-Hill Education.

Dassault Systèmes, 2025. *Abaqus 2025 FDO2 Abaqus/CAE user's guide*. https://www.3ds.com.

Fosroc, 2019. *Nitowrap CW: High performance, high strength carbon fibre system for structural reinforcement of concrete*. https://www.fosroc.com.

Hafezolghorani, M., Hejazi, F., Vaghei, R., Jaafar, M.S. Bin and Karimzade, K., 2017. Simplified damage plasticity model for concrete. In: *Structural Engineering International*. Int. Assoc. for Bridge and Structural Eng. Eth-Honggerberg. pp. 68–78. https://doi.org/10.2749/101686616X1081.

Harvey, P. S. and Cain, T.M.N., 2020. Buckling of elastic columns with initial imperfections and load eccentricity. *Structures*, 23, pp. 660–664. https://doi.org/10.1016/j.istruc.2019.09.021.

Hassoun, M.N. and Al-Manaseer, A., 2020. *Structural concrete: Theory and design*. 7th ed. Hoboken, NJ: John Wiley & Sons, Inc.

Ibrahim, T.H., 2017. Buckling loads and effective length factor for non-prismatic columns. *Journal of Engineering*, 23(10), pp. 431–444. https://doi.org/10.31026/j.eng.2017.10.10.

Kadhim, J.A., Al.Zaidee, S.R. and Al-Baghdadi, H.A., 2025. Seismic performance of reinforced concrete non-prismatic columns. *Journal of Engineering*, 31(7), pp. 53–69. https://doi.org/10.31026/j.eng.2025.07.03.

Korentz, J., 2020. Influence of geometric imperfections on buckling resistance of reinforcing bars during inelastic deformation. *Materials*, 13(16). https://doi.org/10.3390/MA13163473.

Lee, J. and Fenves, G.L., 1998. Plastic-damage model for cyclic loading of concrete structures. *Journal of Engineering Mechanics*, 124(8), pp. 892–900. https://doi.org/10.1061/(ASCE)0733-9399(1998)124:8(892).

Lubliner, J., Oliver, J., Oller, S. and Oñate, E., 1989. A plastic-damage model for concrete. *International Journal of Solids and Structures*, 25(3), pp. 299–326. https://doi.org/10.1016/0020-7683(89)90050-4.

Mahboubi, S. and Shiravand, M.R., 2019. Failure assessment of skew RC bridges with FRP piers based on damage indices. *Engineering Failure Analysis*, 99, pp. 153–168. https://doi.org/10.1016/j.engfailanal.2019.02.010.

Mai, A.D., Sheikh, M.N. and Hadi, M.N.S., 2018. Investigation on the behaviour of partial wrapping in comparison with full wrapping of square RC columns under different loading conditions. *Construction and Building Materials*, 168, pp. 153–168. https://doi.org/10.1016/j.conbuildmat.2018.02.003.

Mercimek, Ö., Ghoroubi, R., Anil, Ö., Çakmak, C., Özdemir, A. and Kopraman, Y., 2020. Strength, ductility, and energy dissipation capacity of RC column strengthened with CFRP strip under axial load. *Mechanics Based Design of Structures and Machines*, 51(2), pp. 961–979. https://doi.org/10.1080/15397734.2020.1860772.

Naqe, A.W. and Al-zuhairi, A.H., 2020. Strengthening of RC beam with large square opening using CFRP. *Journal of Engineering*, 26(10), pp. 123–134. https://doi.org/10.31026/j.eng.2020.10.09.

Narule, G.N. and Bambole, A.N., 2021. An experimental study on axial behavior of CFRP-strengthened RC rectangular columns with variable slenderness ratio. *Asian Journal of Civil Engineering*, 22(2), pp. 263–275. https://doi.org/10.1007/s42107-020-00312-5.

Sadeghian, P. and Fillmore, B., 2018. Strain distribution of basalt FRP-wrapped concrete cylinders. *Case Studies in Construction Materials*, 9. https://doi.org/10.1016/j.cscm.2018.e00171.

Saleh, E., Tarawneh, A., Almasabha, G. and Momani, Y., 2022. Slenderness limit of FRP-confined rectangular concrete columns. *Structures*, 38, pp. 435–447. https://doi.org/10.1016/j.istruc.2022.02.030.

Samy, K., Fouda, M.A., Fawzy, A. and Elsayed, T., 2022. Enhancing the effectiveness of strengthening RC columns with CFRP sheets. *Case Studies in Construction Materials*, 17. https://doi.org/10.1016/j.cscm.2022.e01588.

Shaikh, F.U.A. and Alishahi, R., 2019. Behaviour of CFRP wrapped RC square columns under eccentric compressive loading. *Structures*, 20, pp. 309–323. https://doi.org/10.1016/j.istruc.2019.04.012.

Sudhir Sastry, Y.B., Budarapu, P. R., Krishna, Y. and Devaraj, S., 2014. Studies on ballistic impact of the composite panels. *Theoretical and Applied Fracture Mechanics*, 72(1), pp. 2–12. https://doi.org/10.1016/j.tafmec.2014.07.010.

Tafsirojjaman, T., Ur Rahman Dogar, A., Liu, Y., Manalo, A. and Thambiratnam, D.P., 2022. Performance and design of steel structures reinforced with FRP composites: A state-of-the-art review. *Engineering Failure Analysis*, 138, P. 106371. https://doi.org/10.1016/j.engfailanal.2022.106371.

Walport, F., Gardner, L. and Nethercot, D.A., 2020. Equivalent bow imperfections for use in design by second order inelastic analysis. *Structures*, 26, pp. 670–685. https://doi.org/10.1016/j.istruc.2020.03.065.

Yan, Z.W., Bai, Y.L., Ozbakkaloglu, T., Gao, W.Y. and Zeng, J.J., 2021. Axial impact behavior of Large-Rupture-Strain (LRS) fiber reinforced polymer (FRP)-confined concrete cylinders. *Composite Structures*, 276. https://doi.org/10.1016/j.compstruct.2021.114563.

دراسة عددية لأعمدة خرسانية مسلحة مربعة مقواة بألياف الكربون تحت ضغط محوري مع عيوب هندسية أولية

علي ماجد موسى*، صلاح رحيمة عبيد

قسم الهندسة المدنية، كلية الهندسة، جامعة بغداد، بغداد، العراق

الخلاصة

تُعدّ الأعمدة الخرسانية المسلحة ركيزة أساسية في المدن الحديثة؛ ويتطلب نمذجتها العددية معالجة دقيقة للعيوب الهندسية الأولية وتأثيرات الحصر لتمثيل سلوكها الإنشائي بشكل واقعي. تصف هذه الدراسة إطار عمل لتحليل العناصر المحدودة (FEA) تم تطويره في برنامج Abaqus/CAE، خصيصًا لدراسة السلوك المحوري لأعمدة خرسانية مسلحة مربعة قصيرة ونحيلة بالحجم الطبيعي، مع وبدون تسليح عرضي داخلي (روابط). تتضمن النماذج حصرًا خارجيًا باستخدام غلاف من البوليمر المقوى بألياف الكربون (CFRP)، وتمت دراسة حالات مختلفة من العيوب الكلية والمحلية لتقييم تأثيرها على المقاومة والمطيلية. تمت معايرة النتائج وفقًا لأحكام الكود من خلال مقارنة النتائج العددية بمخطط تفاعلي مُستمد وفقًا لمتطلبات التصميم ACI 318-25 و ACI PRC-440.2-23. أظهرت الدراسة أنه مع ازدياد سعة العيوب، تنخفض مقاومة ومطيلية الأعمدة الخرسانية المسلحة القصيرة والنحيلة، بغض النظر عن الحصر. بالنسبة للأعمدة القصيرة المعرضة لضغط محوري، يمكن تحقيق توافق جيد مع تنبؤات الحمل المحوري الاسمي المستندة إلى الكود دون الحاجة إلى مراعاة العيوب الصريحة، شريطة عدم تضمين عامل تخفيض المقاومة وتجاهل الانحرافات العرضية. في المقابل، بالنسبة للأعمدة النحيلة، تُعد العيوب عاملاً أساسياً في إحداث تأثيرات النحافة، لا سيما في حالات العيوب الكلية ذات شروط الحدود المفصلية.

الكلمات المفتاحية: أعمدة خرسانية محملة محورياً، معايرة قائمة على الكود، تغليف بألياف الكربون المقواة بالبوليمر، العناصر المحدودة، عيوب هندسية أولية.